Table of Contents

Appendix Table S1

Reagent, Antibodies and Virus	SOURCE	IDENTIFIER
Tetrodotoxin (TTX)	Sigma-Aldrich	Cat# 4368-28-9
DL-APV	Tocris	Cat# 0105
CNQX disodium salt hydrate	Tocris	Cat# 1045
SR-95531 (gabazine)	Tocris	Cat# 1262
Adensine 5'-triphosphate magnesium salt	Sigma-Aldrich	Cat# A9187
Guanosine 5'-triphosphate sodium salt	Sigma-Aldrich	Cat# G8877
Lidocaine N-ethyl Bromide (QX-314)	Sigma-Aldrich	Cat# L5783
Phosphocreatine disodium salt hydrate	Sigma-Aldrich	Cat# P7936
Carbachol chloride	Abmole	Cat# 51-83-2
Noradrenaline bitartrate	Abmole	Cat# 108341-18-0
Atropine sulfate	Abmole	Cat# 55-48-1
Mecamylamine hydrochloride (MEC)	Abmole	Cat# 826-39-1
Pirenzepine dihydrochloride	Abmole	Cat# 29868-97-1
4-DAMP	Sigma-Aldrich	Cat# 1952-15-4
Retigabine	Absin	Cat# 150812-12-7
XE991 dihydrochloride	Tocris	Cat# 122955-13-9
Goat-serum	Thermo Fisher	Cat# 16210064
GAD 65	Abcam	Cat# Ab26113
GFP	Abcam	Cat# Ab13970
Alex Fluor 488	Thermo Fisher	Cat# A-11039
Alex Fluor 488	Abcam	Cat# 150113
Gold antifade reagent	ProLong	Cat# 2260877
AAV2/9- hSyn-GCaMP6s	Taitool	Cat# S0528-9-H50
AAV2/9-hSyn-hChR2(H134R)-mCherry	Taitool	Cat# S0312-9-H50
AAV2/9-hSyn-mCherry-WPRE	Taitool	Cat# S0238-9-H20
Corticosterone ELISA Kit	Enzo life sciences	Cat# ADI-900-097
Experimental Models: Strains		
Ai32 mouse: *B6.129S-Gt(ROSA)26Sor*$^{tm32(CAG-COP4*H134R/EYFP)Hze}$*/J*	The Jackson Laboratory	RRID:012569
Ai9 mouse: *B6.Cg-Gt(ROSA)26Sor*$^{tm9(CAG-tdTomato)Hze}$*/J*	The Jackson Laboratory	RRID:007909
PV-cre mouse: *B6.129P2-Pvalb*$^{tm1(cre)Arbr}$*/J*	The Jackson Laboratory	RRID:008069
Software and Algorithms		
Prism	GraphPad	RRID:002798
Mini Analysis	Synaptosoft	RRID:002184

MATLAB R2016a	MathWorks	RRID:001622
BioRender	BioRender	RRID: SCR_018361

Appendix Figures and Figure Legends

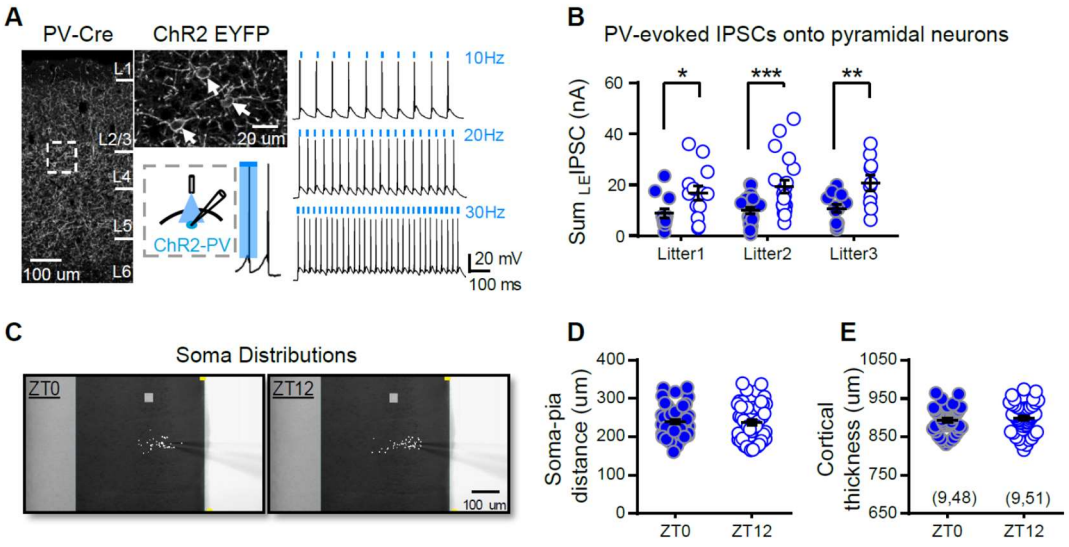

Appendix Figure S1. The strengthened output from PV neurons by the end of the light cycle was neither due to the difference in ChR2 expression nor the spatial distribution of the recorded neurons.

A. Brief blue light reliably activated ChR2-expressed PV neurons (white arrows) in V1. B. Comparison of the sum $_{LE}$IPSC amplitude between ZT0 and ZT12. Mice from the same litter were randomly recorded at either time points and the results were compared within litter (Mann-Whitney U test, Litter 1: ZT0: 9.02 ± 1.83 nC; ZT12: 16.97 ± 2.91 nC; Litter 2: ZT0: 10.07 ± 1.68 nC; ZT12: 19.47 ± 3.24 nC; Litter 3: ZT0: 10.82 ± 1.66 nC; ZT12: 20.82 ± 2.79 nC; *P < 0.05; **P < 0.01; ***P < 0.001). C. The locations of all recorded pyramidal neurons were mapped on the reference image. D. The soma to pia distance of all recorded pyramidal neurons did not differ between ZT0 and ZT12 (ZT0: 239.7 ± 5.72 μm; ZT12: 237.6 ± 6.91 μm; Mann-Whitney U test, P = 0.67). E. The cortical thickness between brain slices used in ZT0 and ZT12 did not differ (ZT0: 892.8 ± 4.64 μm; ZT12: 898.4 ± 5.23 μm; Mann-Whitney U test, P = 0.41). Sample size indicated as (mice, cells).

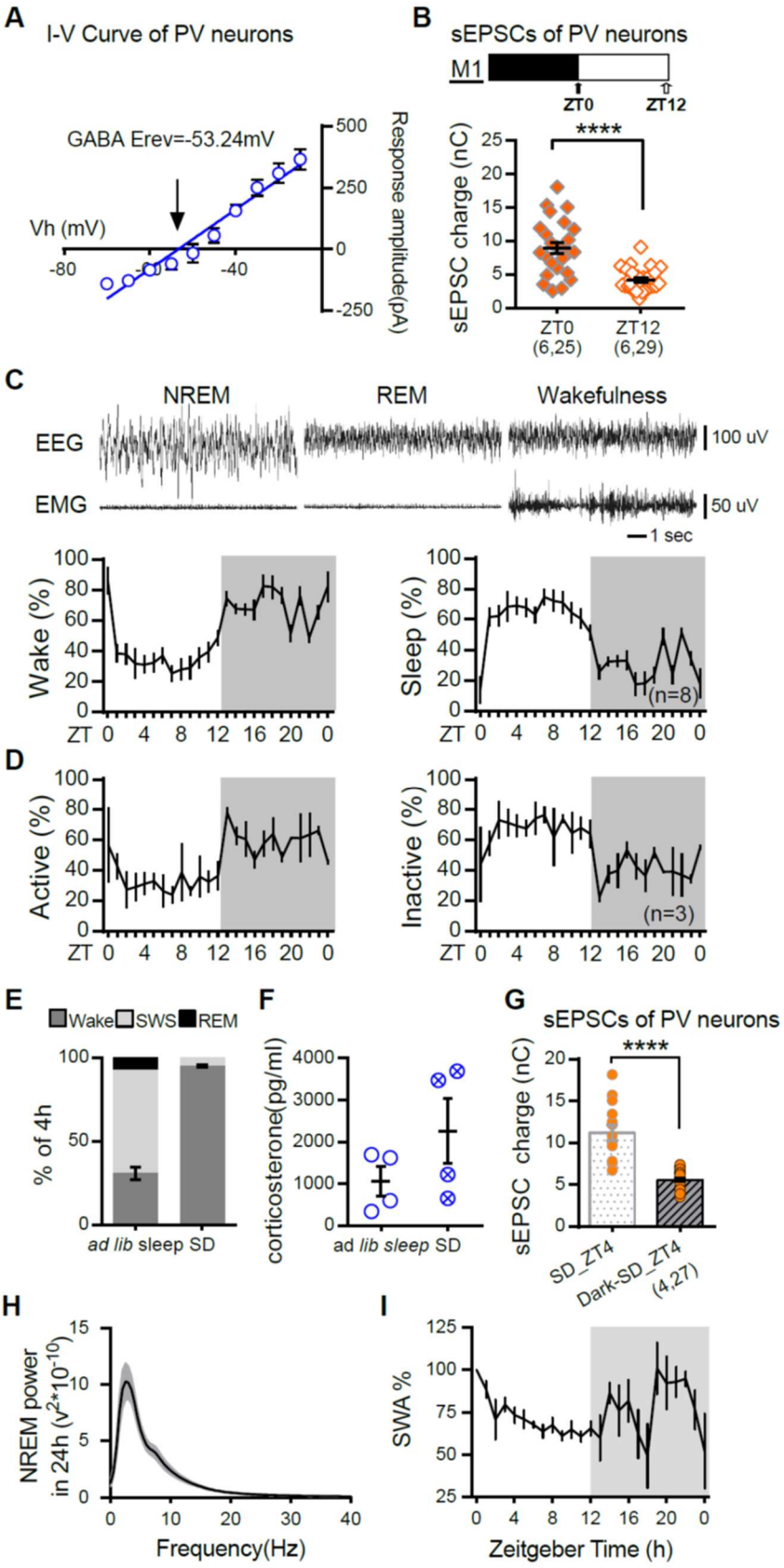
A
I-V Curve of PV neurons
GABA Erev=-53.24mV
Vh (mV)
-80
-40
500
250
0
-250
Response amplitude(pA)
B
sEPSCs of PV neurons
M1
ZT0
ZT12
****
sEPSC charge (nC)
ZT0
(6,25)
ZT12
(6,29)
C
NREM
REM
Wakefulness
EEG
EMG
100 uV
50 uV
1 sec
Wake (%)
Sleep (%)
(n=8)
ZT 0 4 8 12 16 20 0
D
Active (%)
Inactive (%)
(n=3)
E
Wake SWS REM
% of 4h
ad lib sleep SD
F
corticosterone(pg/ml)
ad lib sleep SD
G
sEPSCs of PV neurons
****
sEPSC charge (nC)
SD_ZT4
Dark-SD_ZT4
(4,27)
H
NREM power in 24h (V2*10-10)
Frequency(Hz)
I
SWA %
Zeitgeber Time (h)

Appendix Figure S2. Experience- and sleep-dependent regulation of synaptic transmission of PV neurons.

A. I-V curve obtained with 100 μM APV and 20 μM CNQX in the bath. Reversal potential for GABA receptor was calculated when I is 0. E_{rev}= -53.24 ± 0.65 mV, n = 13 cells. Linear fit R^2 = 0.96. B. PV neurons in L2/3 of the primary motor cortex had higher sEPSCs at ZT0 than ZT12 (ZT0: 8.99 ± 0.82 nC; ZT12: 4.18 ± 0.30 nC; Mann-Whitney U test, P < 0.0001). C. Top: Examples of EEG and EMG signal recorded during NREM, REM sleep and wakefulness. The 24-hour sleep (bottom right panel) and wake (bottom left panel) patterns of PV:Ai9 mice monitored by chronic EEG and EMG recordings. D. The 24-hour activity patterns of PV:Ai9 mice monitored by video. E. EEG and EMG recordings confirmed the efficacy of 4-hour sleep deprivation between ZT0 and ZT4. *Ad lib* sleep group: n = 4; SD group: n = 4 mice. F. 4 hours of sleep deprivation caused variable but not significant changes in plasma corticosterone level (Sleep: 1066 ± 348 pg/ml; SD: 2261 ± 773 pg/ml; Mann-Whitney U test, P = 0.34). G. Sleep deprivation in complete darkness from ZT0 to 4 prevents the increase in sEPSCs induced by SD alone (SD_ZT4 as reported in Fig 3H; Dark-SD_ZT4: 5.57 ± 0.21 nC; Mann-Whitney U test, P < 0.0001). H. The total NREM power spectrum during the 24-hour day. I. Temporal profile of NREM • power during the light/dark cycle.

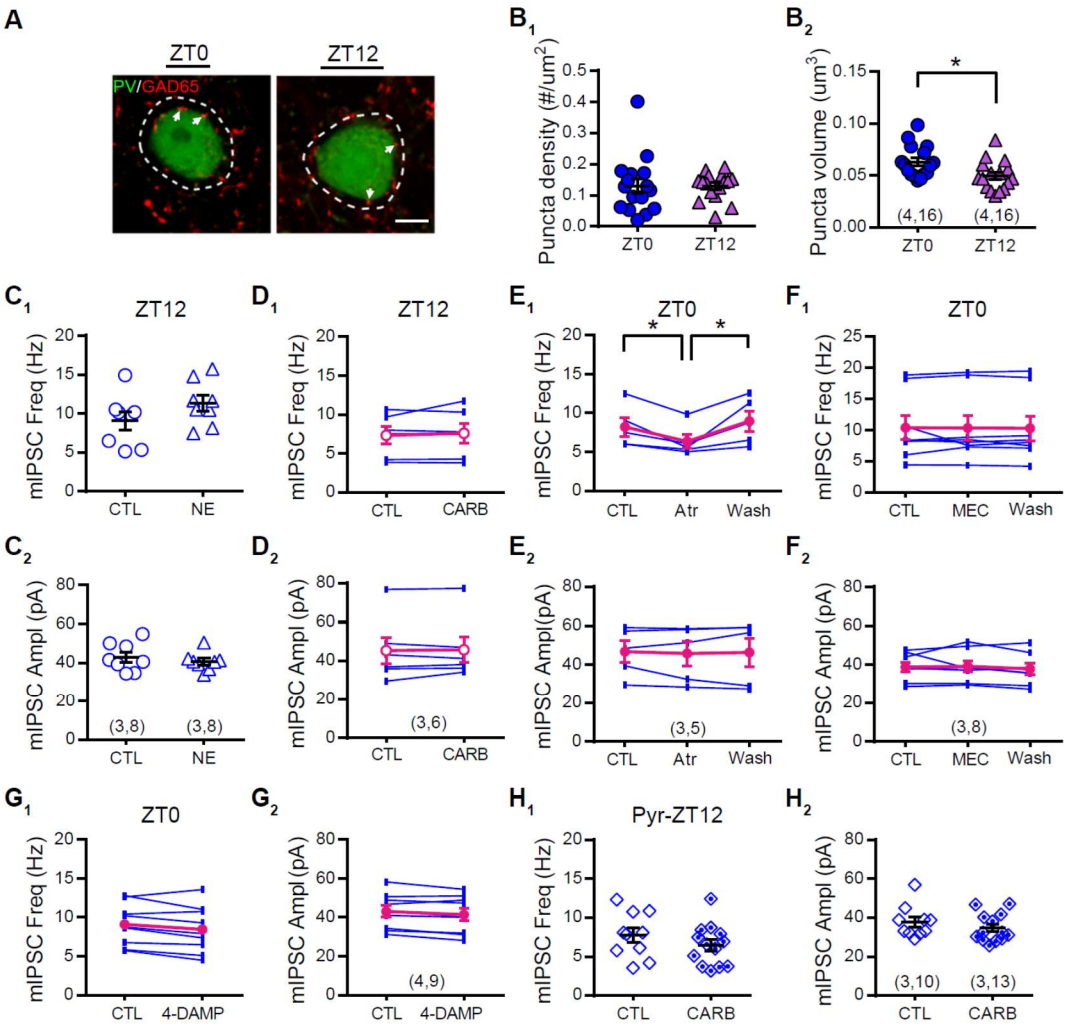

Appendix Figure S3. ACh via M1R specifically regulates mIPSCs of PV neurons.

A. Representative images showing GAD65 staining in PV:Ai9 mice scarified at ZT0 and ZT12 (green: PV neuron; red: GAD65; scale: 10 μm). $B_{1\text{-}2}$, Somatic GAD65-IR puncta density (B_1; ZT0: 0.13 ± 0.02; ZT12: 0.12 ± 0.01; Mann-Whitney U test, P = 0.58) and puncta size (B_2; ZT0: 0.063 ± 0.003; ZT12: 0.049 ± 0.003; Mann-Whitney U test, P = 0.020) around PV neurons. $C_{1\text{-}2}$. Incubation with norepinephrine (NE) was effectless on mIPSC frequency (C_1, CTL: 9.07 ± 1.16 Hz; NE: 11.31 ± 1.01 Hz; Mann-Whitney U test, P = 0.1044) and amplitude (C_2, CTL: 43.03 ± 2.61 pA; NE: 40.68 ± 1.69 pA; Mann-Whitney U test, P = 0.7023) at ZT12. $D_{1\text{-}2}$. Acute infusion with carbachol (CARB) at ZT12 had no effect on mIPSC frequency (D_1, CTL: 7.34 ± 1.13 Hz; CARB: 7.59 ± 1.28 Hz; Wilcoxon signed-rank test, P = 0.78) and amplitude (D_2, CTL: 45.28 ± 6.85 pA; CARB: 45.71 ± 6.58 pA; Wilcoxon signed-rank test, P = 0.99). $E_{1\text{-}2}$. Atropine (Atr) effect on the mIPSC frequency at ZT0 could be reversed by washing out the drug (E_1, CTL: 8.22 ± 1.20 Hz; Atr: 6.37 ± 0.88 Hz; Wash: 8.96 ± 1.32 Hz; One-way repeated measures ANOVA, F (1, 4) = 8.384, P = 0.035). No change in mIPSC amplitude was detected (E_2, CTL: 46.75 ± 5.56 pA; Atr: 45.78 ± 6.40 pA; Wash: 46.24 ± 7.35 pA; One-way repeated measures ANOVA, F (2, 8) = 0.1056, P = 0.90). $F_{1\text{-}2}$. Washing on and out nAChR antagonist *mecamylamine (MEC)*

caused no change in mIPSCs of PV neurons at ZT0 (F_1, frequency, CTL: 10.41 ± 1.89 Hz; MEC: 10.37 ± 1.96 Hz; Wash: 10.30 ± 1.96 Hz; One-way repeated measures ANOVA, F (2, 14) = 0.041, P = 0.95; F_2, amplitude, CTL: 38.90 ± 2.45 pA; MEC: 39.28 ± 2.81 pA; Wash: 37.87 ± 2.82 pA; One-way repeated measures ANOVA, F (2, 14) = 0.66, P = 0.52). $G_{1\text{-}2}$. Infusion of M3R antagonist 4-DAMP had no significant effect on mIPSCs at ZT0 (G_1, frequency; CTL: 9.09 ± 0.88 Hz; 4-DAMP: 8.45 ± 0.99 Hz; Wilcoxon signed-rank test, P = 0.09; G_2, amplitude; CTL: 43.07 ± 3.01 pA; 4-DAMP: 41.44 ± 3.17 pA; Wilcoxon signed-rank test, P = 0.054). $H_{1\text{-}2}$. Incubation with carbachol at ZT12 did not affect the mIPSCs of pyramidal neurons in V1 L2/3 (H_1, frequency; CTL: 7.76 ± 0.92 Hz; CARB: 6.45 ± 0.73 Hz; Mann-Whitney U test, P = 0.34; H_2, amplitude; CTL: 37.76 ± 2.59 pA; CARB: 34.73 ± 2.00 pA; Mann-Whitney U test, P = 0.31). Sample size is indicated as (mice, cells).

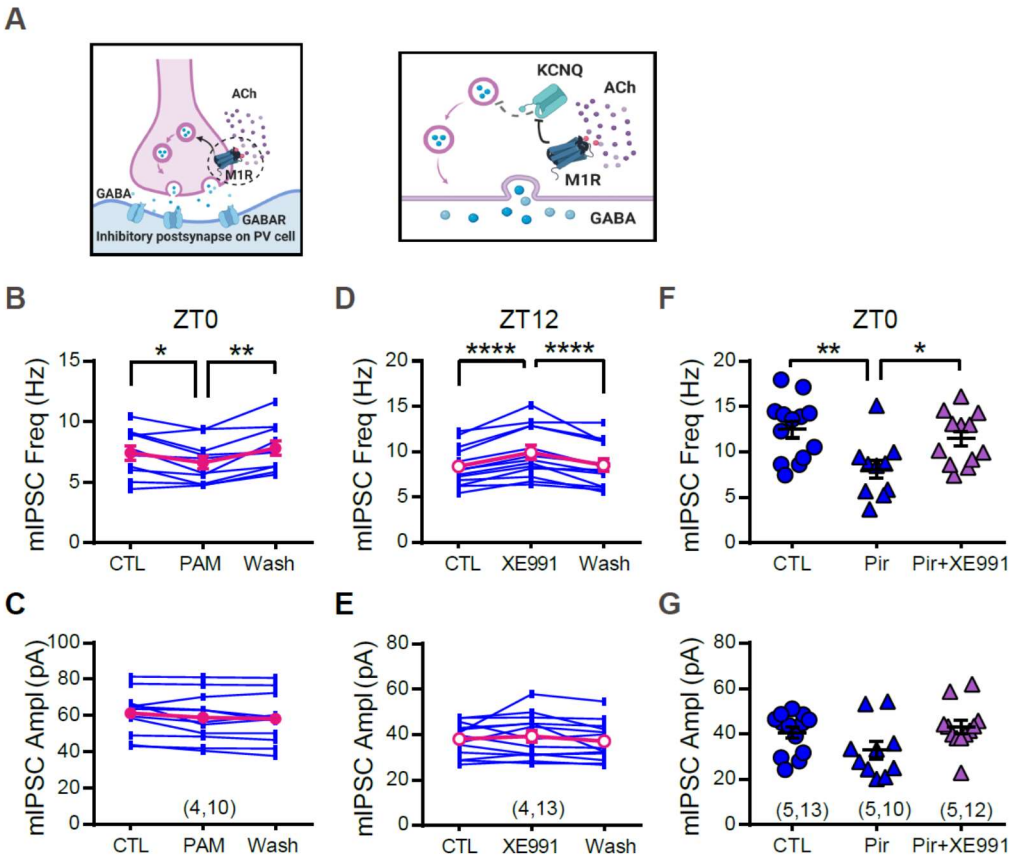

Appendix Figure S4. KCNQ channel is required for the M1R-dependent regulation of inhibitory synaptic transmission of PV neurons.

A. Diagram showing the potential regulatory mechanism of PV's inhibitory synaptic transmission utilizing KCNQ channels and M1R. B-C. The wash-on and wash-off effect of the KCNQ channels allosteric modulator retigabine (PAM) on PV's mIPSC frequency (B, CTL: 7.43 ± 0.62 Hz; PAM: 6.63 ± 0.56 Hz; Wash: 7.82 ± 0.62 Hz; One-way repeated measures ANOVA, F (2, 18) = 6.75, P = 0.007) and amplitude (C, CTL: 59.48 ± 6.27 pA; PAM: 57.88 ± 5.58 pA; Wash: 59.70 ± 6.60 pA; One-way repeated measures ANOVA, F (2, 20) = 3.19, P = 0.06) at ZT0. D-E. The wash-on and wash-off effect of the KCNQ channels blocker XE991 on PV's mIPSC frequency (D, CTL: 8.39 ± 0.60 Hz; XE991: 9.90 ± 0.77 Hz; Wash: 8.52 ± 0.68 Hz; One-way repeated measures ANOVA, F (2, 24) = 18.62, P < 0.0001) and amplitude (E, CTL: 38.01 ± 2.0 pA; XE991: 39.25 ± 2.63 pA; Wash: 37.25 ± 2.34 pA; One-way repeated measures ANOVA, F (2, 24) = 1.11, P = 0.34) at ZT12. F-G. mIPSCs recordings in the presence of pirenzepine (Pir) alone or together with XE991. (F, frequency, CTL: 12.47 ± 0.93 Hz; PIR: 8.08 ± 1.02 Hz; PIR+XE991: 11.47 ± 0.83 Hz; One-way ANOVA, F (2, 32) = 5.795, P = 0.0071; G, amplitude, CTL: 40.49 ± 2.50 pA; PIR: 32.83 ± 3.86 pA; PIR+XE991: 43.13 ± 2.87 pA; One-way ANOVA, F (2, 32) = 2.877, P = 0.071). Datasets were presented as mean ± SEM. Sample size is indicated as (mice, cells).

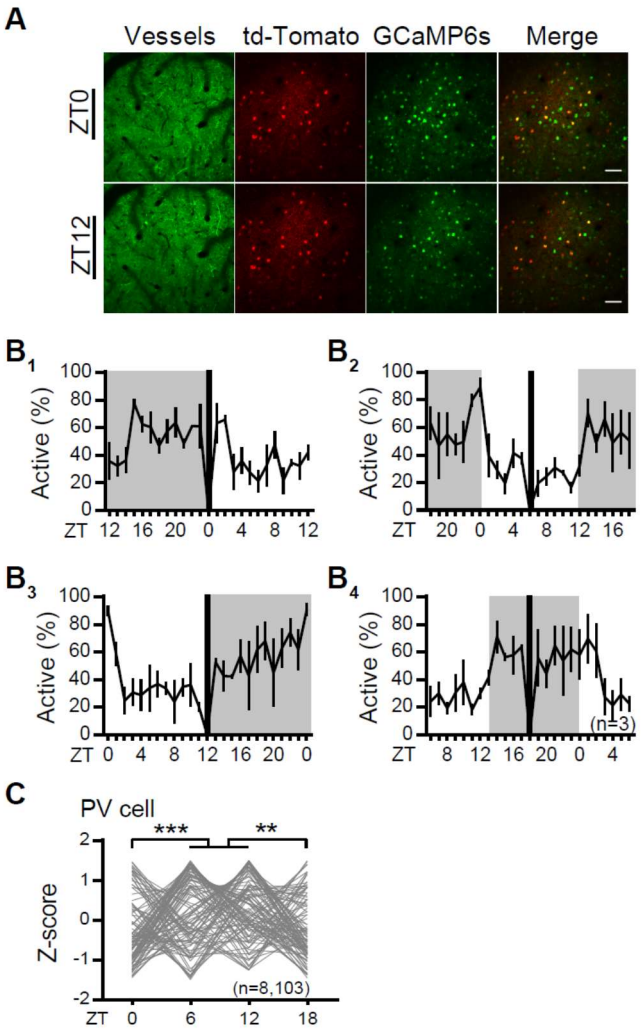

Appendix Figure S5. Daily oscillation in PV's spontaneous activity correlates with mice's sleep/wake cycle.

A. Same population of PV neurons were repetitively imaged at different times of the day by using vascular features, td-Tomato and GCaMP6s signals as markers. Scale bar: 100 μm. $B_{1\text{-}4}$. Pre- and post- 12h arousal states of mice imaged at ZT0, ZT6, ZT12 and ZT18. Regular activity cycles were maintained. C. Activity of individual PV neurons imaged repetitively at four time points (ZT0: -0.26 ± 0.08; ZT6: 0.21 ± 0.09; ZT12: 0.26 ± 0.07; ZT18: -0.21 ± 0.07; One-way repeated measures ANOVA, $F(3, 300) = 8.586$, $P < 0.0001$).

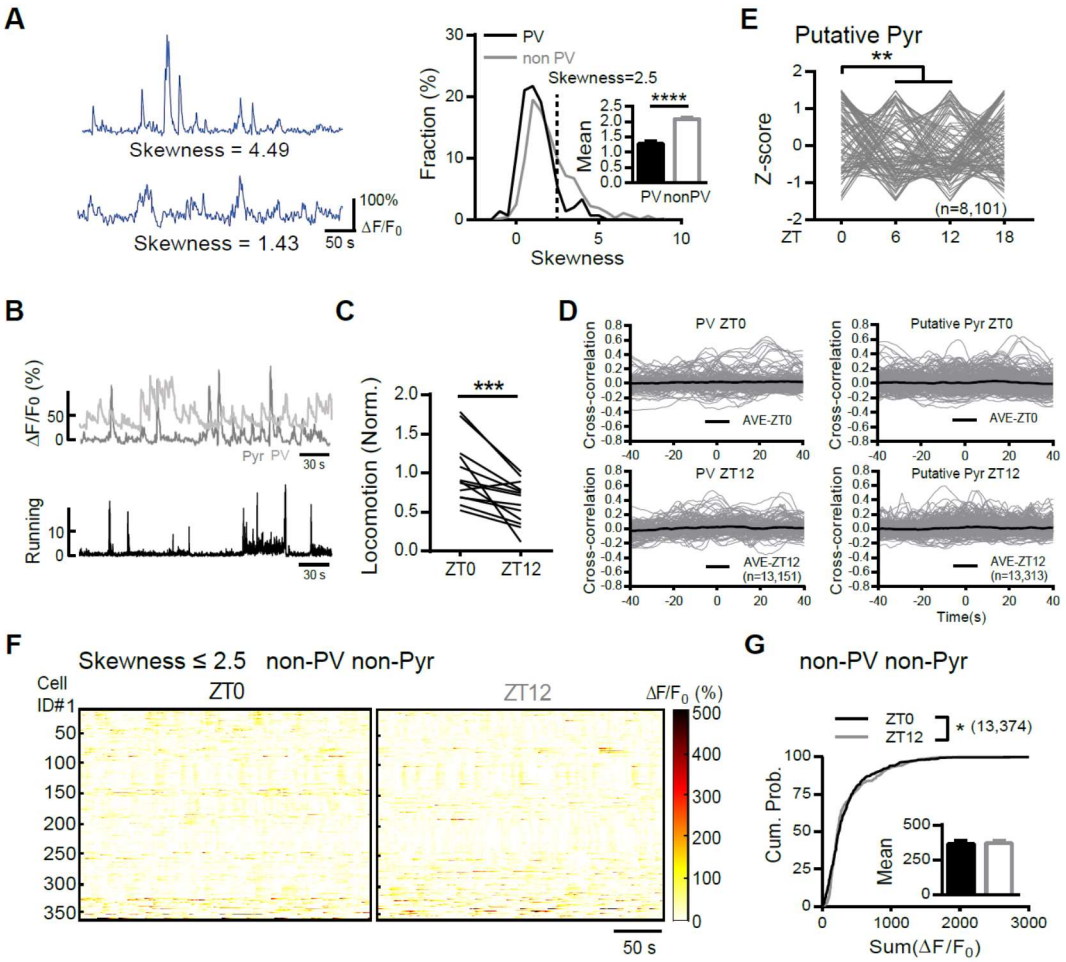

Appendix Figure S6. PV and putative pyramidal neurons daily oscillations did not correlate with locomotor activity.

A. Representative •F/F_0 traces and their corresponding skewness from a putative pyramidal neuron (left top) and PV neuron (left bottom). Right panel, Distribution of skewness of PV (black) and non-PV (gray) neurons. Inset: the mean skewness (PV: 1.26 ± 0.08; non-PV: 2.08 ± 0.05). B. Top, representative •F/F_0 traces from one PV neuron (light gray) and one putative pyramidal neuron (dark gray) from the same field of view. Bottom, trace showing the instantaneous running speed of the mouse. C. The normalized locomotor activity of all mice during both imaging sections (ZT0: 1.0 ± 0.11; ZT12: 0.62 ± 0.07). D. The cross correlation between the •F/F_0 of individual neuron and the locomotor activity at ZT0 and ZT12 (left panels: PV neurons; right panels: putative pyramidal neurons). E. Activity of individual putative pyramidal neurons imaged repetitively at four time points (ZT0: 0.24 ± 0.09; ZT6: -0.14 ± 0.08; ZT12: -0.17 ± 0.07; ZT18: 0.07 ± 0.08; One-way repeated measures ANOVA, F (3, 400) = 5.494, P = 0.001). F. Heatmaps showing the spontaneous •F/F_0 time-series of all non-PV, non-pyramidal cells imaged at ZT0 and ZT12. G. The cumulative distribution of the sum •F/F_0 of all non-PV, non-pyramidal cells imaged at ZT0 (black) and ZT12(gray) (*K-S* test, P = 0.027). Inset, the means of sum •F/F_0 (ZT0: 363.9 ± 22.27; ZT12: 370.8 ± 19.85 um; P = 0.75). Sample size indicated as (mice, cells).

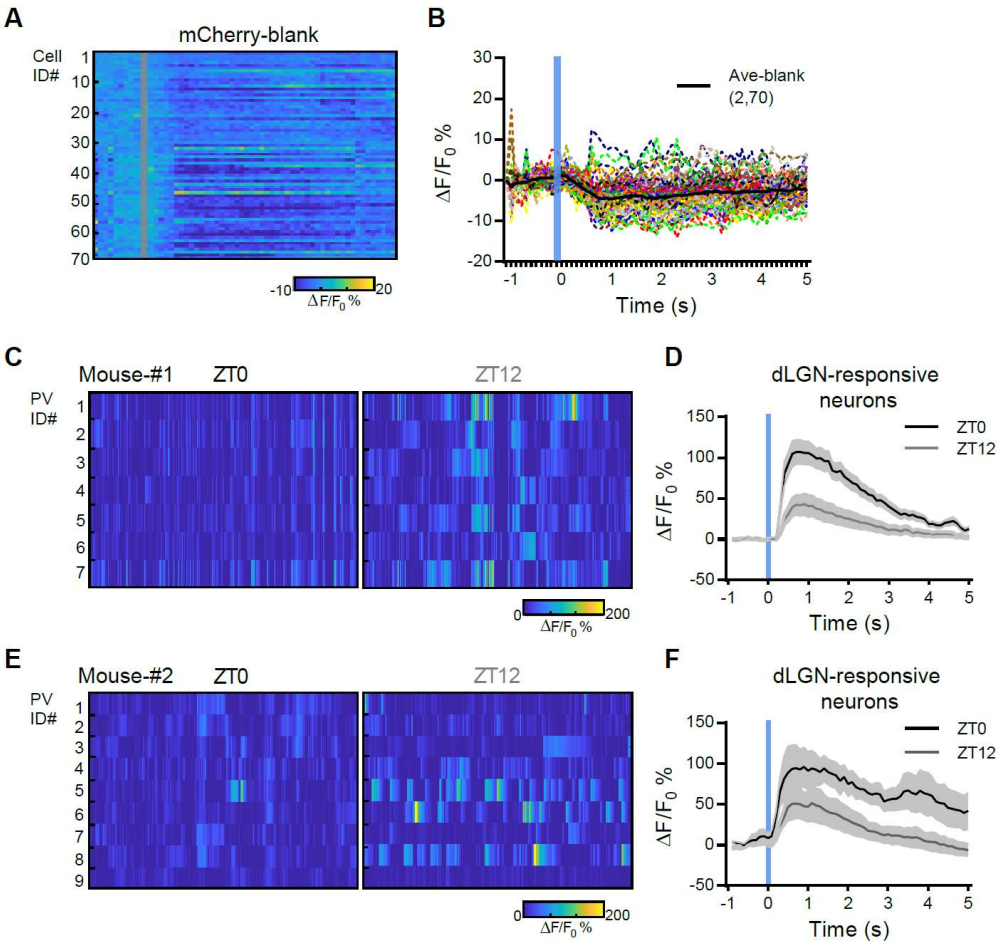

Appendix Figure S7. Absence of dLGN-evoked response in mice expressing mCherry-blank virus in dLGN.

A. Heatmap showing Ca^{2+} signal upon dLGN light stimulation in mouse expressing mCherry-blank virus in dLGN. Trials were aligned to LED onset time (gray solid lines). B. The mean Ca^{2+} response (•F/F_0%) waveforms of all neurons (dotted color lines) within the field of view during all trials of stimulation. The black solid line represents the averaged waveform of all neurons. The vertical blue line indicates stimulus onset time. C-F. Left panels, heatmaps showing the spontaneous activity of PV neurons at ZT0 (left) and ZT12 (right) in mouse #1 (C) and #2(E) during the 5 min prior the onset of the dLGN stimulation. Right panels, mean Ca^{2+} response (•F/F_0%) waveforms from all dLGN-responsive neurons in the same FOV of PV neurons at ZT0 (black trace) and ZT12 (gray trace) from mouse #1 (C) and #2(E).

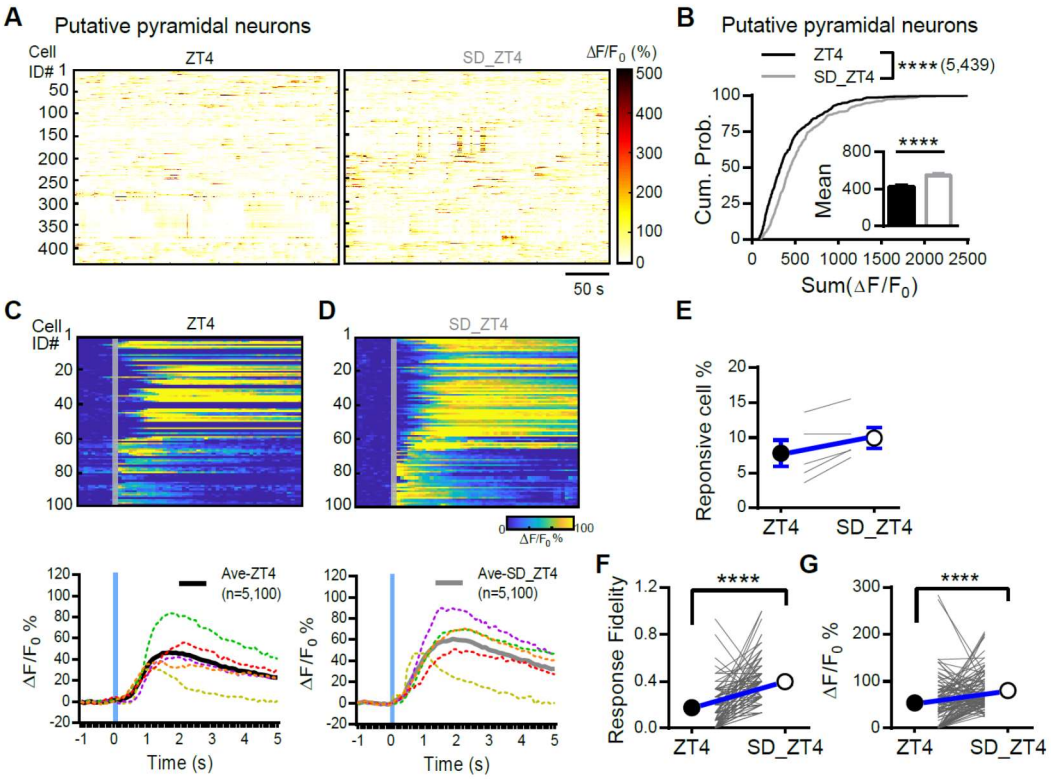

Appendix Figure S8. 4 hours of sleep deprivation increased spontaneous neural activity of putative pyramidal neurons and augmented dLGN-evoked responses in V1.

A. Heatmaps showing the spontaneous •F/F_0 time-series traces of all putative pyramidal neurons imaged at ZT4 and SD_ZT4. The color code represents the magnitude of •F/F_0(%). B. Cumulative probability distribution of the sum •F/F_0 of all putative pyramidal neurons imaged at ZT4 and SD_ZT4 (*K-S* test; $P < 0.0001$). Inset: the mean sum •F/F_0 (ZT4: 427.5 ± 15.72; SD_ZT4: 550.2 ± 17.87; $P < 0.0001$; Mann-Whitney U test). C-D. Top: color-coded calcium signals of all responsive neurons (% •F/F_0). Bottom: The mean Ca^{2+} response waveform from individual mouse (dotted color lines) and all mice (thick black and gray lines). Trials were aligned to LED onset time (gray solid lines). E. The fraction of neurons responsive to dLGN stimuli at ZT4 and SD_ZT4. Each gray line represents one mouse. Black and white circles and error bars represent the mean and SEM (ZT4: 7.8 ± 1.86; SD_ZT4: 9.95 ± 1.49; $P = 0.125$; Wilcoxon signed-rank test; n = 5 mice). F. The Response fidelity of each cell at ZT4 and SD_ZT4. Black and white circles and error bars represent the mean and SEM (ZT4: 0.17 ± 0.017; SD_ZT4: 0.39 ± 0.018; $P < 0.0001$; Wilcoxon signed-rank test; n = 100 cell). G. Comparison of the evoked response amplitude of each cell at ZT4 and SD_ZT4. Black and white circles and error bars represent the mean and SEM (ZT4: 53.97 ± 5.23; SD_ZT4: 80.43 ± 4.03; $P < 0.0001$; Wilcoxon signed-rank test; n = 100 cell). Sample size is indicated as (mice, cells).